DETECTION OF GASTRIC CANCER RISK FROM X-RAY IMAGES VIA PATCH-BASED CONVOLUTIONAL NEURAL NETWORK

Kenta Ishihara, Takahiro Ogawa and Miki Haseyama

Graduate School of Information Science and Technology, Hokkaido University
N-14, W-9, Kita-ku, Sapporo, 060-0814, Japan
Email: {ishihara, ogawa}@lmd.ist.hokudai.ac.jp, miki@ist.hokudai.ac.jp

ABSTRACT

This paper presents a novel detection method of gastric cancer risk from X-ray images using the patch-based Convolutional Neural Network (CNN). Our method enables the training of the patch-based CNN which can accurately detect gastric cancer risk even though there is only the image-level ground truth. Furthermore, the proposed method can extract a feature vector that can represent the whole of symptoms associated with the presence or absence of the risk. Specifically, the proposed method selects the patches related to their true risk via the CNN, and it is the most innovative contribution of our method. Moreover, we extract the feature vector by applying the Bag-of-Feature representation to the output values from the CNN's intermediate layer obtained from the selected patches. Finally, the detection of gastric cancer risk is performed by inputting the extracted feature vector into Support Vector Machine. Experimental results confirm that the proposed method outperforms a previously reported method that combines the detection results obtained from X-ray images taken from multiple angles even though the proposed method only uses an X-ray image taken from a single angle, and we can achieve a higher performance than that of doctors.

Index Terms— Convolutional neural network, Bag-of-Features, gastric cancer risk detection, X-ray image.

1. INTRODUCTION

Chronic atrophic gastritis triggered by Helicobacter pylori (H. pylori) infection causes the development of gastric cancer [1–3], and gastric cancer risk is decreased by H. pylori eradication therapy [4]. Therefore, gastric cancer mass screening is actively executed by focusing on not only detection of gastric cancer but also detection of its risk, *i.e.,* H. pylori infection and chronic atrophic gastritis.

For gastric cancer mass screening, a diagnostic imaging such as X-ray examination and endoscopy is necessary. Although the detection rate of gastric cancer by endoscopy is twice higher than that of X-ray examination [5], the endoscopy cannot be applied to a large number of patients since it has the performance limitation of the operation number [6]. If more efficient and accurate X-ray examination becomes feasible, the X-ray examination will be utilized as an alternative examination to endoscopy until the number of endoscopists increase or more efficient endoscopy is developed. For the efficient and accurate X-ray examination, Computer-Aided Diagnosis (CAD) systems that automatically analyze X-ray images are useful for decreasing diagnosis time and preventing doctors' overlooking.

For realizing the CAD systems, we have proposed the detection methods of gastric cancer risk from X-ray images [7–9]. These methods utilizing the handcraft features achieved the accuracy close to that of the X-ray examination doctors. For more accurate detection of gastric cancer risk, the introduction of Convolutional Neural Network (CNN) [10] will be effective since the methods with CNN significantly outperformed the handcraft feature-based methods as previously reported in [11, 12]. Actually, much medical imaging literature has been published in which the detection methods that show superior performance by using CNN are proposed [13]. When CNN is applied to the high resolution images such as medical images, the patch-based CNN is adopted [14, 15] instead of directly applying CNN to these images to avoid the high computational cost of CNN. However, for introducing the patch-based CNN into the detection method of gastric cancer risk, we have the following two problems:

(Problem 1)
Since there is only the image-level ground truth (GT) for gastric cancer risk, *i.e.,* there is not GT for the individual patches, it is necessary to train CNN from only the patches related to the presence or absence of gastric cancer risk.

(Problem 2)
Since our goal is to decide whether the patient has the gastric cancer risk or not from X-ray images, it is necessary to obtain the image-level detection result from multiple patches.

In this paper, we propose a new detection method of gastric cancer risk from X-ray images using the patch-based CNN to overcome the above problems. Our contribution of this paper is twofold:

(Contribution 1)
For overcoming **Problem 1**, we select the patches related to the presence or absence of gastric cancer risk, *i.e.,* the patches related to their image-level GT, by extracting the relevant scores between each patch and the image-level GT.

(Contribution 2)
For overcoming **Problem 2**, we calculate features that can represent the characteristics of the whole symptoms associated with the presence or absence of gastric cancer risk from the patches selected by **Contribution 1**.

In **Contribution 1**, the relevant scores between each patch and the image-level GT are extracted from the probabilities obtained from the patch-based CNN's output layer, and we apply thresholding to

In this research, we utilized image data and results that were kindly provided by the Medical Examination Center of Yamagata City Medical Association. We would also like to sincerely thank Katsuhiro Mabe of Hakodate National Hospital, Shigemi Nakajima of Japan Community Health care Organization Shiga Hospital, Harufumi Oizumi of Yamagata City Medical Association, Kazuya Yoshizawa of the Faculty of Medicine, Yamagata University, and many others for providing data, images and results as well as invaluable advice. This work was partly supported by JSPS KAKENHI Grant Number JP17H01744.

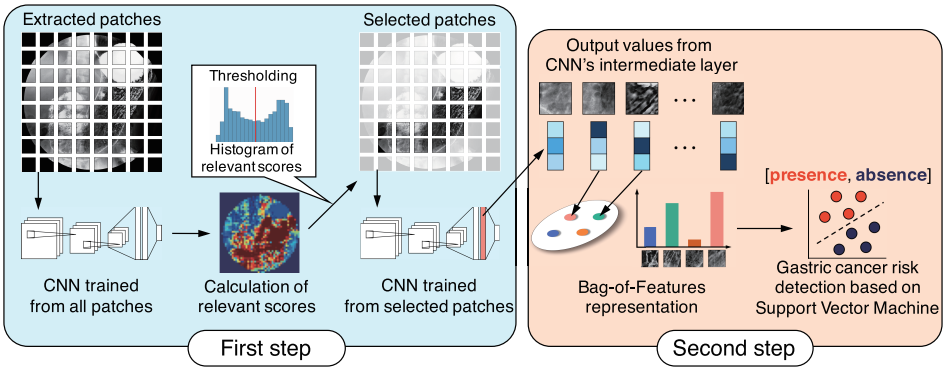

Fig. 1. Overview of our method for detecting gastric cancer risk via patch-based CNN.

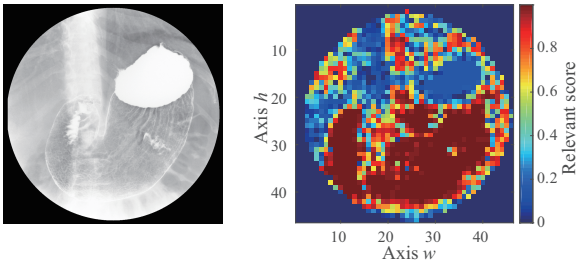

(a) (b)

Fig. 2. Examples of an X-ray image and relevant scores: (a) a real X-ray image and (b) relevant scores calculated from the patches. Note that since the patches including the outside black region shown in (a) are excluded, we set these relevant scores to zero in (b).

these scores to select the patches related to their image-level GT. Furthermore, we retrain CNN from the selected patches. By realizing **Contribution 1**, we can train the patch-based CNN without the GT for individual patches, which enables accurate detection of gastric cancer risk. In **Contribution 2**, we extract the image-level feature vector by applying the Bag-of-Features (BoF) [16] representation to the selected patches' feature vectors obtained from the intermediate layer in CNN. Finally, we obtain the image level detection result by classifying the image-level feature vector. Since the selected patches' feature vectors obtained from CNN effectively represent the various symptoms in the local gastric region related to the presence or absence of the risk, we can obtain the image-level feature that represents the whole symptoms by extracting the distribution of these features based on the BoF representation. Consequently, accurate detection of the gastric cancer risk becomes feasible.

2. DETECTION OF GASTRIC CANCER RISK VIA PATCH-BASED CNN

In this section, the gastric cancer risk detection method using the patch-based CNN is explained. We show the overview of the proposed method in Fig. 1. As shown in Fig. 1, the proposed method is composed of two steps, and **Contribution 1** and **Contribution 2** are realized in the first and second steps, respectively. In 2.1, we derive the relevant scores between each patch and the image-level GT and confirm whether the patches related to their image-level GT are extracted based on these scores. In 2.2, we explain the first step that selects patches related to their image-level GT and retrains CNN using the selected patches as shown in the left side of Fig. 1. In 2.3, we explain the second step in which the image-level gastric cancer detection is performed by extracting feature vector from the selected patches as shown in the right side of Fig. 1.

2.1. Derivation of Relevant Scores

The objective of this subsection is the derivation of the relevant scores and the visual verification of the effectiveness of using the patch-based CNN outputs for obtaining the relevant score. In Fig. 2, we show an X-ray image and the relevant scores extracted from the image. As we can observe in Fig. 2, the relevant scores on the stomach region are higher than those on its outside region. Each patch's relevant score $r^{(h,w)}$ ($(h,w) = (1,1),(1,2),\cdots,(2,1),\cdots,(H,W)$; (h,w) being an axis of these patches) is derived as follows:

$$r^{(h,w)} = |p_+^{(h,w)} - p_-^{(h,w)}|, \tag{1}$$

where $p_+^{(h,w)}$ and $p_-^{(h,w)}$ are the probabilities of the presence of gastric cancer risk and the absence of the risk, respectively. By inputting each patch into the patch-based CNN that has already learned, the probabilities $p_C^{(h,w)} (C \in \{+,-\})$ are calculated as follows:

$$p_C^{(h,w)} = \frac{\exp(z_C^{(h,w)})}{\sum_{k \in C} \exp(z_k^{(h,w)})}, \tag{2}$$

where $z_C^{(h,w)}$ is the input to the unit C of the CNN's output layer for patch (h,w). The CNN is trained from the sets of the patches obtained from X-ray images that differ from Fig. 2 (b) and their image-level GT.

In the training of the patch-based CNN, we use all patches including the patches obtained from an area unrelated to their image-level GT such as the outside of stomach. Although these unrelated areas exist regardless of the presence or absence of gastric cancer risk, *i.e.,* they are visually similar, the GT of the patch extracted from these area is different among X-ray images since we assign the image-level GT to the patches on the training of CNN. Therefore, the differences between $p_+^{(h,w)}$ and $p_-^{(h,w)}$ obtained from the patch become close to zero, compared with the patch related to their image-level

GT. From the above reason, we can extract the patches related to their image-level GT by utilizing the relevant scores between each patch and the image-level GT. In other words, we can select the patches related to their image-level GT from the relevant scores if we calculate an appropriate threshold to decide whether or not the patches are related to their image-level GT.

2.2. Training of Patch-based CNN via Selection of Patches

The first step is composed of the following three processes: (i) training of CNN from all patches, (ii) selection of patches related to their image-level GT, and (iii) retraining of CNN from the selected patches.

(i) Training of CNN from all patches
Given N gastric X-ray images whose presence or absence of gastric cancer risk is already known, *i.e.,* training data, the proposed method divides ith ($i = 1, 2, \cdots, N$) X-ray image into multiple patches $\boldsymbol{X}_i^{(h,w)}$. Furthermore, the proposed method trains CNN using the sets of patches $\boldsymbol{X}_i^{(h,w)}$ and their image-level GT, *i.e.,* its presence or absence of gastric cancer risk.

(ii) Selection of patches related to their image-level GT
As discussed in 2.1, we calculate an appropriate threshold to decide whether or not the patches are related to their image-level GT. The proposed method inputs all patches $\boldsymbol{X}_i^{(h,w)}$ into CNN trained in process (i) to obtain the probabilities $p_{i+}^{(h,w)}$ and $p_{i-}^{(h,w)}$, which are calculated based on Eq. (2). Furthermore, we calculate the relevant score $r_i^{(h,w)}$ based on Eq. (1). Although we ideally expect the relevant scores to be zero in the outside of stomach, in practice, they are noisy as shown in Fig. 1 (a). For the calculation of the appropriate threshold, we reduce the noise generated on the outside of stomach by calculating an average of the relevant scores $r_i^{(h,w)}$ for each $(h, w)((h, w) = (1, 1), (1, 2), \cdots, (2, 1), \cdots, (H, W))$ as follows:

$$\bar{r}^{(h,w)} = \frac{1}{N} \sum_{i=1}^{N} r_i^{(h,w)}.$$

By applying Otsu's method [17] to the obtained average score $\bar{r}^{(h,w)}$, we calculate the appropriate threshold T to decide whether or not the patches are related to the image-level GT. By using the calculated threshold T, the proposed method can select the patches $\boldsymbol{X}_i^{(h,w)}$ satisfying $r_i^{(h,w)} \geq T$ as those related to their image-level GT.

(iii) Retraining of Patch-based CNN from selected patches
The proposed method retrains CNN by using the sets of the selected patch and its image-level GT. When we apply the above processes to an X-ray image whose true label is unknown, *i.e.*, test data, the proposed method divides the image into $H \times W$ patches and inputs these patches into CNN trained in process (i). Then we can obtain the probabilities $p_+^{(h,w)}$ and $p_-^{(h,w)}$ from each patch, which respectively mean the probabilities of presence and absence of gastric cancer risk. The proposed method calculates the relevant score $r^{(h,w)}$ and selects the patches satisfying $r^{(h,w)} \geq T$ as the patches related to their true risk. From these processes, we can train the patch-based CNN that can accurately detect gastric cancer risk without using individual patches' GT by selecting the patches related to their image-level GT.

2.3. Image-level Detection from Selected Patches

In the second step, we perform image-level detection of gastric cancer risk by extracting a new feature vector from multiple patches selected in process (ii) of subsection 2.2. For extracting a new feature vector, the proposed method utilizes the output values from the patch-based CNN's intermediate layer trained in process (iii) of subsection 2.2. These output values obtained by inputting the selected patch to trained CNN represent the local feature of X-ray image since each patch is local region of the image. Furthermore, the symptoms associated with presence or absence of gastric cancer risk appear on the various parts of stomach such as mucosal surface pattern, fold distribution and fold shape [18]. However, even though these patches' positions are the same among the images, the region of the stomach and the symptoms photographed into these patches are slightly different due to the differences of the gastric size and shape between patients. Therefore, the proposed method applies the BoF representation to the output values from the CNN's intermediate layer. By utilizing the BoF representation, we can consider the differences of the gastric size and shape between patients and represent the distribution of the whole of the symptoms. Finally, we perform image-level detection of gastric cancer risk by classifying the feature vector via Support Vector Machine (SVM) [19].

When we obtain an X-ray image whose gastric cancer risk is unknown, *i.e.*, test data, we obtain the output values from the CNN's intermediate layer by inputting the selected patches to CNN according to the aforementioned procedure. The proposed method applies the BoF representation to these output values obtained from all of the selected patches. Furthermore, we can obtain the image-level detection result by inputting the obtained feature vector to the trained SVM. Consequently, the accurate detection of gastric cancer risk becomes feasible by extracting the feature vector that represents the characteristics of the whole symptoms associated with gastric cancer risk.

3. EXPERIMENTAL RESULTS

3.1. Experimental Conditions

In this experiment, we used X-ray images taken from 2,100 patients. Each patient's GT was obtained from a blood examination [20]. From the blood examination, 1,129 patients were considered to be without gastric cancer risk (negative patients) and 971 patients were regarded as having the risk (positive patients). Furthermore, each image was of 8-bit gray scale and had a resolution of $1,024 \times 1,024$ pixels. In order to confirm the effectiveness of the selection of the patches related to their image-level GT and the feature extraction from the selected patches, the following comparative methods were adopted.

(1) Comparative method 1 (CM1) only applies the first step of the proposed method to the extracted patches. The image-level detection result is obtained by combining the detection results of the selected patches based on majority voting.

(2) Comparative method 2 (CM2) classifies all patches by utilizing CNN trained from all patches, *i.e.,* CM2 does not calculate the relevant score between each patch and the image-level GT. The image-level detection result is obtained by combining the detection results of all patches based on majority voting.

(3) Comparative method 3 (CM3) applies the same framework as that of the proposed method to the handcraft features shown in Table 1. Specifically, we replace CNN of the proposed method with the classification of the handcraft feature based on logistic regression.

Table 1. Features extracted in comparative method 3.

Feature description	Dimension
Intensity histogram-related features	4
Co-occurrence matrix-related features [21]	9
Gabor Wavelet-based features	56
Adaptive Local Binary Patterns	22
Hu-moment invariant [22]	7
Hough transform [23]-based features	2
Sobel filter [24]-based edge features	1
Total dimension	101

Table 2. The architecture of CNN in this experiment. The output size is given in width×height×the number of feature maps. Conv, Max-pool and Fc represent convolutional, max pooling and fully-connected layers. ReLU [25] function was used for all Conv and Fc layers' activation function. The dropout [26] was used between Fc and Output, whose probability was set to 0.5.

Layer type	Filter size, stride	Output size
Input	-	100×100×1
Conv	5×5, 1	96×96×20
Max-pool	3×3, 2	48×48×20
Conv	5×5, 1	44×44×50
Max-pool	3×3, 2	22×22×50
Conv	5×5, 1	18×18×50
Max-pool	3×3, 2	9×9×50
Fc	-	100
Output	2	2

(4) Comparative method 4 (CM4) is our previous method [7]. This method focuses on the characteristic of X-ray examination on which X-ray images are generally taken from multiple angles per patient. Concretely, this method obtains multiple detection results by utilizing handcraft features extracted from X-ray images taken from multiple angles and integrates these results considering the accuracy of each angle's classifier. Note that the classifier is the Gaussian kernel-based SVM whose parameters obtained via grid search. The details of the used handcraft features are denoted in [7, 9].

(5) Comparative method 5 (CM5) only uses single angle's classifier constructed in CM4, *i.e.,* this method does not integrate multiple detection results. Note that the used X-ray images are the same as those of the proposed method.

Note that the proposed method, CMs1-3 and CM5 only used X-ray images taken from a single angle, *i.e.,* total number of X-ray images was 2,100. On the other hand, CM4 used X-ray images taken from eight angles, *i.e.,* total number of X-ray images was 2,100×8. Furthermore, in the proposed method and CMs1-3, we set the size of the patch and its overlapping size to 100×100 pixels and 20 pixels, respectively. Consequently, H and W became 46, and the total number of patches became 3,038,281. Note that the patches including the outside black region as shown in Fig. 2 (b) were excluded from analyzing targets in this paper. The architecture of CNN is shown in Table 2. Furthermore, the network was constructed via the Caffe framework [27] on a single NVidia Tesla 80K GPU. The number of bins for the BoF representation was experimentally set to 1,000, and their centroid vectors were calculated by an on-line k-means algorithm [28]. In the proposed method and CM3, the linear kernel was used for the kernel function in second step's SVM, whose regularized parameter was set to one[1].

Table 3. Sensitivity (Se), specificity (Sp) and harmonic mean of sensitivity and specificity (Ha) in the proposed method (PM) and the comparative methods.

	PM	CM1	CM2	CM3	CM4	CM5
Se	**0.895**	0.828	0.588	0.631	0.869	0.734
Sp	0.935	0.964	**0.984**	0.671	0.873	0.855
Ha	**0.914**	0.890	0.730	0.649	0.870	0.788

The verification method was 10-fold cross-validation. We computed the following evaluation criteria: sensitivity (Se=TP/(TP+FN)), specificity (Sp=TN/(TN+FP)) and harmonic mean of sensitivity and specificity (Ha=(2×Se×Sp)/(Se+Sp)). TP, TN, FP and FN represent the numbers of true positive, true negative, false positive and false negative, respectively. Furthermore, Welch's t-test was applied to Ha obtained from 10-fold cross-validation as a significant difference test.

3.2. Results and Discussion

We show the results of all methods in Table 3. As shown in Table 3, sensitivity and harmonic mean of the proposed method were higher than those of all comparative methods. The results of the Welch's t-test confirmed the statistically significant ($p < 0.05$) performance of the proposed method against all comparative methods. Comparison between the proposed method and CM2 shows the effectiveness of the selection scheme of the patches related to their image-level GT based on the relevant scores. Moreover, from comparison between the proposed method and CM1, we can confirm that the proposed method can extract more discriminative features by applying the BoF representation to the CNN's output values obtained from the selected patches. Since the proposed method outperformed CMs3-5 in terms of all evaluation criteria, the use of CNN was very effective for the detection of the gastric cancer risk. It should be specially mentioned that although CM4 utilized X-ray images taken from multiple angles, the proposed method only used X-ray image taken from a single angle. It is reported that the sensitivity and specificity of the doctors are 0.932 and 0.867, respectively when focusing on the blood examination as the GT [18]. The above results suggest that the proposed method has higher detection performance than that of doctors since the doctors' Ha is 0.898 calculated from the above reports.

4. CONCLUSIONS

We have proposed a novel detection method for gastric cancer risk from X-ray images by utilizing the patch-based CNN. Our method enables the accurate detection by selecting the patches related to their true risk and extracting the image-level features from these patches. The proposed method outperforms the method that integrates the detection results obtained from multiple X-ray images even though the proposed method only uses a single X-ray image. Therefore, we will improve the detection performance by integrating multiple detection results obtained from the proposed method in the future.

[1]Note that although we also used the Gaussian kernel-based SVM whose parameters obtained via grid search, the performance of the proposed method was rarely different from that of the linear kernel-based SVM.

5. REFERENCES

[1] N. Uemura, S. Okamoto, S. Yamamoto, N. Matsumura, S. Yamaguchi, M. Yamakido, K. Taniyama, N. Sasaki, and R. J. Schlemper, "Helicobacter pylori infection and the development of gastric cancer," *New England Journal of Medicine*, vol. 345, no. 11, pp. 784–789, 2001.

[2] H. Ohata, S. Kitauchi, N. Yoshimura, K. Mugitani, M. Iwane, H. Nakamura, A. Yoshikawa, K. Yanaoka, K. Arii, H. Tamai, Y. Shimizu, T. Takeshita, O. Mohara, and M. Ichinose, "Progression of chronic atrophic gastritis associated with helicobacter pylori infection increases risk of gastric cancer," *Int. Journal of Cancer*, vol. 109, no. 1, pp. 138–143, 2004.

[3] H. Watabe, T. Mitsushima, Y. Yamaji, M. Okamoto, R. Wada, T. Kokubo, H. Doi, H. Yoshida, T. Kawabe, and M. Omata, "Predicting the development of gastric cancer from combining helicobacter pylori antibodies and serum pepsinogen status: a prospective endoscopic cohort study," *Gut*, vol. 54, no. 6, pp. 764–768, 2005.

[4] K. Fukase, M. Kato, S. Kikuchi, K. Inoue, N. Uemura, S. Okamoto, S. Terao, K. Amagai, S. Hayashi, and M. Asaka, "Effect of eradication of helicobacter pylori on incidence of metachronous gastric carcinoma after endoscopic resection of early gastric cancer: an open-label, randomized controlled trial," *The Lancet*, vol. 372, no. 9636, pp. 392–397, 2008.

[5] K. Sugano, "Screening of gastric cancer in asia," *Best Practice & Research Clinical Gastroenterology*, vol. 29, no. 6, pp. 895–905, 2015.

[6] M. Kato and M. Asaka, "Recent development of gastric cancer prevention," *Japanese Journal of Clinical Oncology*, vol. 42, no. 11, pp. 987–994, 2012.

[7] K. Ishihara, T. Ogawa, and M. Haseyama, "Helicobacter pylori infection detection from multiple X-ray images based on decision level fusion," in *Proc. IEEE Int. Conf. Image Processing*, 2014, pp. 2769–2773.

[8] K. Ishihara, T. Ogawa, and M. Haseyama, "Helicobacter pylori infection detection from multiple X-ray images based on combination use of support vector machine and multiple kernel learning," in *Proc. IEEE Int. Conf. Image Processing*, 2015, pp. 4728–4732.

[9] K. Ishihara, T. Ogawa, and M. Haseyama, "Classification of gastric cancer risk from X-ray images based on efficient image features related to serum Hp antibody level and serum PG levels," *ITE Trans. Media Technology and Applications*, vol. 4, no. 4, pp. 337–348, 2016.

[10] Y. Lecun, L. Bottou, Y. Bengio, and P. Haffner, "Gradient-based learning applied to document recognition," in *Proc. the IEEE*, 1998, vol.86, pp. 2278–2324.

[11] A. Krizhevsky, I. Sutskever, and G. E. Hinton, "Imagenet classification with deep convolutional neural networks," in *Proc. Advances in Neural Information Processing Systems 25*, 2012, pp. 1097–1105.

[12] C. Szegedy, W. Liu, Y. Jia, P. Sermanet, S. Reed, D. Anguelov, D. Erhan, V. Vanhoucke, and A. Rabinovich, "Going deeper with convolutions," in *Proc. IEEE Conf. Computer Vision and Pattern Recognition*, 2015, pp. 1–9.

[13] N. Tajbakhsh, J. Y. Shin, S. R. Gurudu, R. T. Hurst, C. B. Kendall, M. B. Gotway, and J. Liang, "Convolutional neural networks for medical image analysis: Full training or fine tuning?," *IEEE Trans. Medical Imaging*, vol. 35, no. 5, pp. 1299–1312, 2016.

[14] Y. Zhou, H. Chang, K. Barner, P. Spellman, and B. Parvin, "Classification of histology sections via multispectral convolutional sparse coding," in *Proc. IEEE Conf. Computer Vision and Pattern Recognition*, 2014, pp. 3081–3088.

[15] Y. Xie, X. Kong, F. Xing, F. Liu, H. Su, and L. Yang, "Deep voting: A robust approach toward nucleus localization in microscopy images," in *Proc. Medical Image Computing and Computer-Assisted Intervention*, 2015, pp. 374–382.

[16] G. Csurka, C. R. Dance, L. Fan, J. Willamowski, and C. Bray, "Visual categorization with bags of keypoints," *In Workshop on Statistical Learning in Computer Vision*, pp. 1–22, 2004.

[17] N. Otsu, "A threshold selection method from gray-level histograms," *IEEE Trans. Systems, Man and Cybernetics*, vol. 9, no. 1, pp. 62–66, 1979.

[18] S. Nakajima, M. Yamaoka, K. Doi, and M. Nishimura, "Barium X-ray characteristics of the stomach with or without h. pylori infection and the diagnostic value," *Japanese Journal of Helicobacter Research*, vol. 8, no. 2, pp. 18–21, 2007. (in Japanese).

[19] C. Cortes and V. Vapnik, "Support-vector networks," *Machine Learning*, vol. 20, no. 3, pp. 273–297, 1995.

[20] K. Miki, "Gastric cancer screening by combined assay for serum anti-Helicobacter pylori IgG antibody and serum pepsinogen levels – "ABC method"," in *Proc. the Japan Academy Series B, Physical and Biological Sciences*, 2011, pp. 405–414.

[21] R. Haralick, K. Shanmugam, and I. Dinstein, "Textural features for image classification," *IEEE Trans. Systems, Man and Cybernetics*, vol. 3, no. 6, pp. 610–621, 1973.

[22] M.-K. Hu, "Visual pattern recognition by moment invariants," *IRE Trans. Information Theory*, vol. 8, no. 2, pp. 179–187, 1962.

[23] R. O. Duda and P. E. Hart, "Use of the hough transformation to detect lines and curves in pictures," *Commun. ACM*, vol. 15, no. 1, pp. 11–15, 1972.

[24] W. Gao, X. Zhang, L. Yang, and H. Liu, "An improved sobel edge detection," in *Proc. IEEE Int. Conf. Computer Science and Information Technology*, 2010, vol.5, pp. 67–71.

[25] V. Nair and G. E. Hinton, "Rectified linear units improve restricted boltzmann machines," in *Proc. Int. Conf. Machine Learning*, 2010, pp. 807–814.

[26] N. Srivastava, G. Hinton, A. Krizhevsky, I. Sutskever, and R. Salakhutdinov, "Dropout: A simple way to prevent neural networks from overfitting," *Journal of Machine Learning Research*, vol. 15, pp. 1929–1958, 2014.

[27] Y. Jia, E. Shelhamer, J. Donahue, S. Karayev, J. Long, R. Girshick, S. Guadarrama, and T. Darrell, "Caffe: Convolutional architecture for fast feature embedding," *arXiv preprint arXiv:1408.5093*, 2014.

[28] D. Sculley, "Web-scale k-means clustering," in *Proc. the 19th Int. Conf. World Wide Web*, 2010, pp. 1177–1178.